FUDMA Journal of Sciences (FJS)
ISSN online: 2616-1370
ISSN print: 2645 - 2944
Vol. 9 April Special Issue, 2025, pp 216 - 223
DOI: https://doi.org/10.33003/fjs-2025-09(AHBSI)-3435

KINETICS OF PHOTOCATALYTIC DEGRADATION OF METHYL ORANGE USING CuO-α-Fe_2O_3 NANOCOMPOSITE UNDER VISIBLE LIGHT IRRADIATION

***[1]Muhammad Suleiman Darma, [2]Abdulhamid Hamza and [3]Ibrahim Imrana**

[1]Department of Chemistry, Federal University Dutsin-Ma, Katsina State. Nigeria.
[2]Department of Chemical Engineering, Ahmadu Bello University, Zaria. Kaduna State.
[3]Department of Pure and Applied Chemistry, Usman Danfodio University, Sokoto State.

*Corresponding authors' email: smdarma@fudutsinma.edu.ng Phone: +2348036392465

ABSTRACT

The treatment of textile azo dyes in wastewater has posed a significant challenge for decades due to their remarkable chemical, photolytic, and microbiological stability. This research focuses on developing a CuO-α-Fe_2O_4 nanocomposite, which provides an efficient method for converting visible light energy into the breakdown of $-N=N-$ linkages found in azo dyes. This process not only mitigates the hazards associated with these materials but also facilitates the essential color removal required in wastewater treatment. To enhance the optical properties and increase the surface area of the CuO-α-Fe_2O_4 nanocomposite, the co-precipitation method was employed during its synthesis. The microstructure, crystallinity and morphology of the nanocomposite were characterized using X-ray diffraction (XRD), and scanning electron microscopy (SEM). A photocatalytic activity test was performed using methyl orange as a model azo dye. The results shows that the CuO-α-Fe_2O_4 composite exhibited excellent photocatalytic activity, achieving a degradation rate of up to 71.6%. In contrast, the degradation rates for CuO and α-Fe_2O_3 were significantly lower, at 26.4% and 34.8% respectively. Kinetic study of the reaction revealed that the catalytic activity followed pseudo-first-order reaction model. These findings highlight the potential of the CuO-α-Fe_2O_4 nanocomposite as an effective solution for azo dye degradation in wastewater treatment. By leveraging its superior photocatalytic activity, this nanocomposite can significantly improve the efficiency of dye removal processes, making it a promising candidate for addressing the environmental challenges posed by textile wastewater.

Keywords: CuO-α-Fe_2O_3, Methyl orange, Photocatalysis, Waste water, Visible light, Irradiation

INTRODUCTION

Due to the growing concern about residual color, which is strongly related with toxicity and aesthetics of the released effluent, color removal has become a difficult part of textile wastewater treatment. (Singh, Bharose, Verma, & Singh, 2013). Under anoxic circumstances, azo dyes, which make up a large amount of the dye industry and have the least desired environmental repercussions, are easily converted to potentially toxic aromatic amines. The most commonly used physico-chemical methods includes coagulation, adsorption, membrane filtration etc, and biochemical method such as aerobic biological treatment for decolorization are often ineffective. This could be because, the commercial textile dyes are purposefully designed to have a high degree of chemical, photolytic, and microbial stability in order to meet the consumption requirements. (Taylor et al., 2014). The treatment ability of textile azo dyes and dye house effluent using various sophisticated chemical oxidation processes has already been thoroughly investigated. (Darma et. Al., 2019). The term "photocatalysis" has Greek origins, consisting of two parts: the prefix "photo," meaning light, and "catalysis," which refers to the process of breaking apart or decomposing substances. Although there are ongoing debates regarding the precise definition of photocatalysis within the scientific community, the term "photocatalyst" is widely accepted. A photocatalyst influences the rate of a chemical reaction without being consumed in the process. This terminology describes a phenomenon where light activates a material to facilitate a reaction. The primary difference between a traditional thermal catalyst and a photocatalyst lies in their activation methods (Auwal et. Al., 2023). A thermal catalyst is activated by heat, while a photocatalyst requires photons of specific energy to initiate the reaction. This distinction is crucial for understanding how photocatalysis operates and its potential applications (Darma et. Al., 2019). Photocatalysis has earned significant attention due to its potential in various fields, including environmental remediation, energy conversion, and chemical synthesis. For instance, photocatalysts can decompose pollutants in water and air, offering a sustainable solution for environmental challenges (Auwal et. Al., 2023). Researchers are actively exploring various materials to enhance photocatalytic efficiency. Titanium dioxide (TiO_2) is one of the most commonly studied photocatalyst because of its stability, non-toxicity, and strong oxidizing power (Kabo et al., 2023). However, its efficiency is limited to ultraviolet light, which constitutes only a small fraction of the solar spectrum. Consequently, scientists are investigating alternative materials and methods to broaden the light absorption range of photocatalysts. Recent advancements include the development of doped photocatalysts, which involve adding impurities to TiO_2 to enable it to absorb visible light. Another approach is the creation of hybrid photocatalysts that combine different materials to optimize performance. These innovations aim to improve the efficiency of photocatalytic reactions and extend their applicability in real-world scenarios (Kumari et, al., 2023). The integration of photocatalysis into various technologies holds promise for addressing some of today's pressing issues. For example, photocatalytic processes can be employed in self-cleaning surfaces, where contaminants are decomposed upon exposure to light. This feature not only enhances cleanliness but also reduces the need for chemical cleaning agents, promoting environmental sustainability (Hamza et. Al., 2017).

MATERIALS AND METHODS

Copper (II) chloride dihydrate, ferric chloride, and sodium hydroxide pellets were all analytical-grade reagents sourced from Sigma-Aldrich in England. These reagents were used without additional purification. Distilled water was employed throughout the synthesis. The Copper (II) chloride dihydrate serves as a source of copper ions, while ferric chloride contributes iron (III) ions to the reactions. Sodium hydroxide acts as a strong base, facilitating the formation of the metals hydroxides from which the CuO-α-Fe_2O_3 nanocomposite if formed.

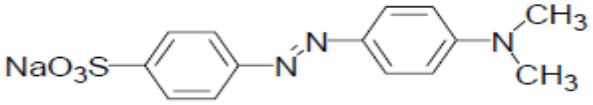

Figure 1: Molecular structure of methyl orange

Preparation of CuO-α-Fe_2O_3 nanocomposite

The co-precipitation method was employed to synthesize the CuO-α-Fe_2O_3 nanocomposite. A 500 ml of distilled water was mixed with 8.50 g of $CuCl_2 \cdot 2H_2O$ and 27.0 g of $FeCl_3 \cdot 6H_2O$. To raise the pH to approximately 10, a concentrated NaOH solution (5 mol/dm³) was added dropwise to the stirring mixture at room temperature. The mixture was stirred continuously for one hour and then heated to 100°C for an additional two hours. After this process, the precipitate was thoroughly washed with distilled-deionized water to eliminate any excess NaCl from the composite mixture. Subsequently, the product was dried in an oven at 100°C and calcined in a furnace at 600°C for two hours (Darma et al., 2019).The systematic reaction scheme of the synthesis is depicted in the figures 2.

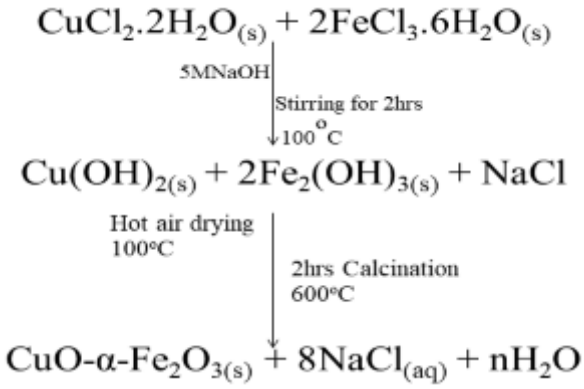

Figure 2: Schematic reaction equations for the synthesis of $CuO - \alpha - Fe_2O_3$ nanocomposite

Characterization

The crystalline phases and crystallite sizes of the $CuO - \alpha - Fe_2O_3$nanocomposite were determined using X-ray diffraction (XRD) analysis conducted with a PAN Analytical Philips diffractometer from England. Energy dispersive X-ray fluorescence spectroscopy was employed to reveal the elemental composition. Additionally, scanning electron microscopy (SEM) analysis from a PHENON PROX (800-07334) spectrophotometer was used to investigate the microscopic structure and surface morphology. The XRD analysis provided insights into the crystalline structure of the nanocomposite. By examining the diffraction patterns, we identified various crystalline phases present within the sample. The crystallite size was calculated using the Scherrer equation, which relates the broadening of the diffraction peaks to the size of the crystallites. This information is crucial for understanding the material's properties and its potential applications. However, we could observe the distribution of particles and any significant features that might influence the material's performance. This morphological information is vital, as it can affect the mechanical and thermal properties of the nanocomposite (Auwal et al., 2023).

Photocatalytic activity test

A predetermined (0.2 g) quantity of the $CuO - \alpha - Fe_2O_3$ nanocomposite powder was added to an aqueous solution containing 30 mg/L Methyl Orange (MO). The suspension was stirred in the dark for 60 minutes to establish adsorption-desorption equilibrium on the $CuO - \alpha - Fe_2O_3$ nanocomposite's surface. After this period, the suspension was exposed to visible light from a 500W halogen lamp. Analytical samples were collected at various irradiation intervals, specifically at 15-minute increments, and analyzed using a UV-Vis spectrophotometer at the maximum absorption peak of 465 nm. This process was designed to evaluate the effectiveness of the nanocomposite in adsorbing and degrading the dye under visible light exposure. By measuring the absorbance at the specified wavelength, we could determine the concentration of MO remaining in the solution over time. The experimental set up is depicted in the figure 3. And hence, the MO removal efficiency was calculated using the equation 1.

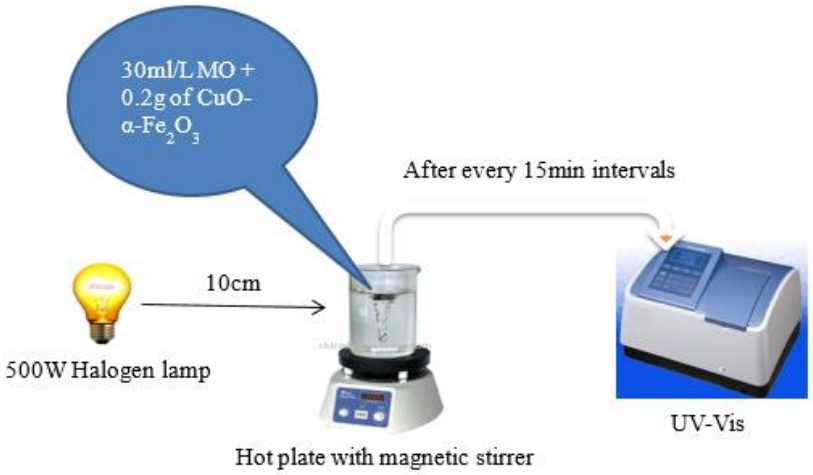

Figure 3: Experimental set up for the Photocatalytic degradation of MO dye

$$Removal\ efficiency = \frac{A_0 - A_t}{A_0} \times 100\% (1)$$

Where A_0 and A_f are the initial MO absorbance in the solution at irradiation time (t).

Comparative study of pure CuO, α-Fe_2O_3 and CuO-α-Fe_2O_3 nanocomposite

This experiment aimed to evaluate the effectiveness of three photocatalysts: pure Copper (II) oxide (CuO), haematite iron oxide (α-Fe_2O_3), and a nanocomposite of CuO-α-Fe_2O_3 for the degradation of methyl orange. All tests were conducted under identical conditions: a methyl orange concentration of 30 mg/L, a photocatalyst dosage of 0.2 g, and a pH of 6. These controlled parameters ensured the reliability of the results. CuO has been extensively studied for its photocatalytic properties, making it a well-known candidate in various degradation processes. Its ability to absorb light and generate reactive species contributes significantly to its effectiveness as a photocatalyst. On the other hand, α-Fe_2O_3 is recognized for its unique advantages, such as abundance and cost-effectiveness, which make it an attractive alternative in photocatalytic applications. The CuO-α-Fe_2O_3 nanocomposite is designed to leverage the strengths of both materials. The combination of CuO and α-Fe_2O_3 aims to enhance photocatalytic activity through synergistic effects. The interaction between the two oxides may improve charge separation and reduce electron-hole recombination, leading to increased photocatalytic efficiency (Umar *et, al.,* 2020).

RESULTS AND DISCUSSION

Table 1: The result of methyl orange degradation using the CuO- α-Fe_2O_3 nanocomposite

Run	Time (min)	MO Conc. (Abs)
1	0.0	0.824
2	15.0	0.769
3	30	0.531
4	45.0	0.422
5	60.0	0.315
6	75.0	0.269
7	90.0	0.251

Table 2: Results of the Comparative tests for the photocatalytic activities of CuO, Fe_2O_3 and the $Cu - \alpha - Fe_2O_3$

RUN	TIME (min)	$Cu - \alpha - Fe_2O_3$	CuO	Fe_2O_3
1	0.0	0.829	0.829	0.829
2	15.0	0.733	0.801	0.801
3	30.0	0.501	0.769	0.733
4	45.0	0.412	0.725	0.685
5	60.0	0.290	0.690	0.602
6	75.0	0.285	0.682	0.573
7	90.0	0.282	0.660	0.555

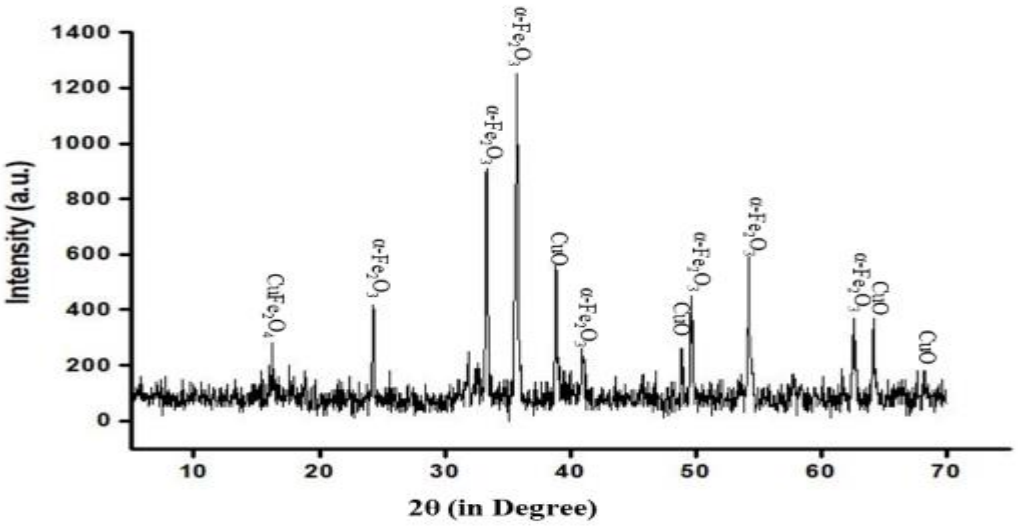

Figure 4: X-ray diffraction spectrum (XRD) of the $Cu-\alpha-Fe_2O_3$ nanocomposite

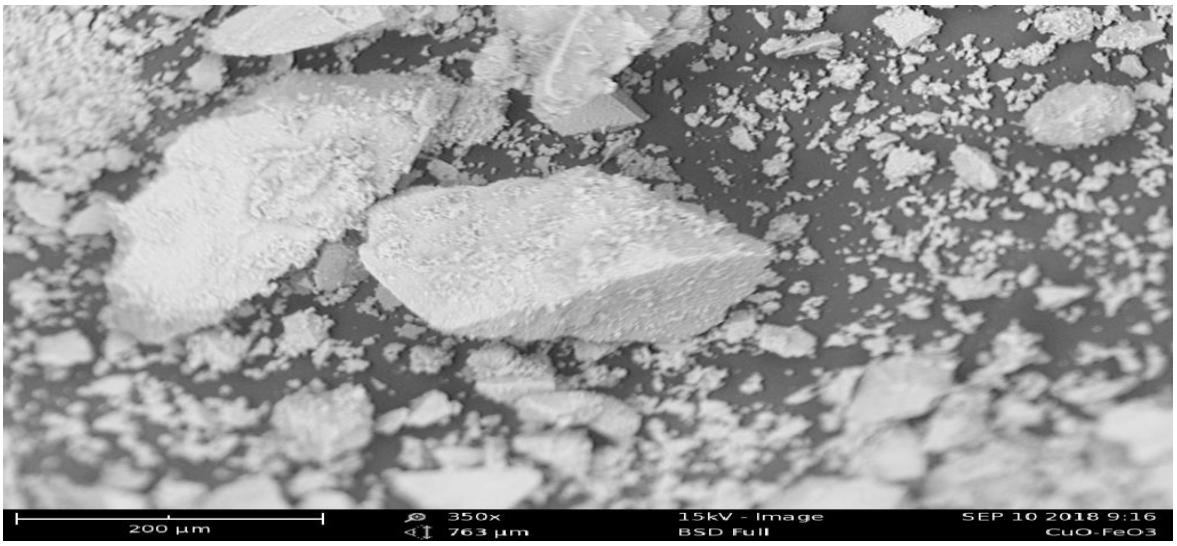

Figure 5: SEM image of the $Cu-\alpha-Fe_2O_3$ nanocomposite

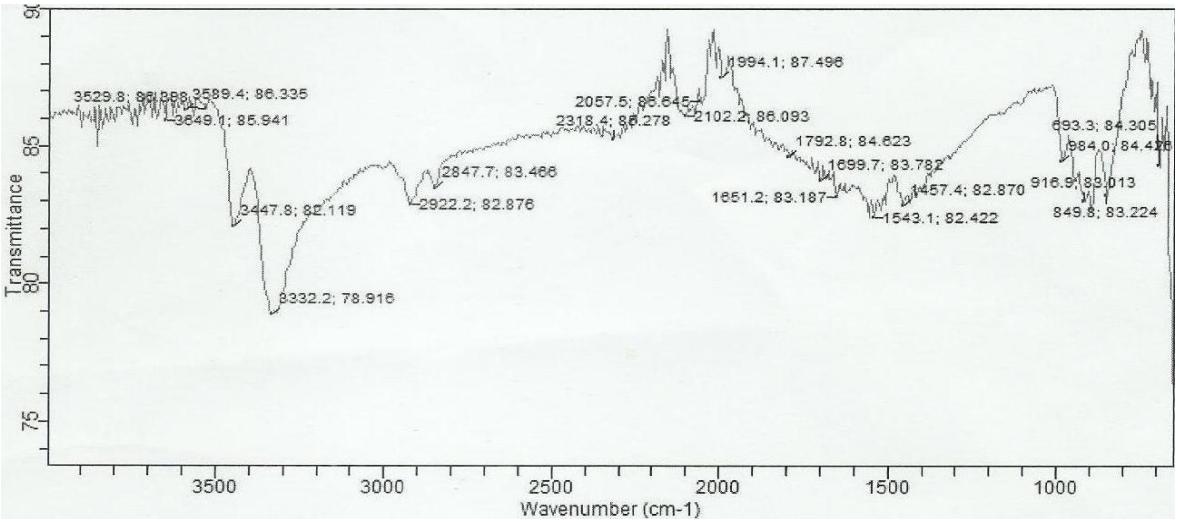

Figure 6: FTIR spectrum of the$CuO-\alpha-Fe_2O_3$ showing the absorption peaks

Characterization

Figure 4 presents the X-ray diffraction (XRD) pattern of the nanocomposite, which exhibits significant diffraction peaks at Bragg's angles (2θ) of 24.40°, 33.20°, 40.90°, 49.50°, 54.20°, and 62.60°. These peaks correspond to the characteristic peaks of the hematite phase of $\alpha - Fe_2O_3$ (JCPDS file No. 33-0664) and demonstrates a rhombohedra symmetry (Hamza et al., 2013). Additionally, the sample shows characteristic diffraction peaks at 2θ values of 39.40°, 43.60°, 56.30°, 57.60°, 64.80°, and 69.80°. These peaks are attributed to monoclinic CuO nanoparticles, and similar results were reported by Chen et al., (2016) (JCPDS File No. 05-0661). Furthermore, the peaks observed at 2θ values of 16.40°, 35.70°, 58.50°, and 64.00° indicates the formation of copper ferrite at the calcination temperature (Darma et al., 2019). The crystalline sizes parameters of the$Cu - \alpha - Fe_2O_3$ nanocomposite are K=0.94, λ=0.1540nm, Θ =35.7º β=(Θ_2-Θ_1)π/180 = (35.9º-35.5º)(0.01746) = 0.006984 as obtained from the XRD analytical data. Computing the crystalline particle sizes using Scherer's equation shows that, the$Cu - \alpha - Fe_2O_3$ nanocomposite exhibited particulate sizes of 25.5nm. The sizes of the composite particles (less than 100nm), have proven the nanoparticulate nature of the prepared $Cu - \alpha - Fe_2O_3$ nanocomposite(Abdulhamid Hamza, John, & Mukhtar, 2017).

The scanning electron microscopy (SEM) images of the synthesized $Cu - \alpha - Fe_2O_3$nanocomposite are presented in Figure 5. These images illustrate the non-uniform crystalline arrangements and varied geometries of the $Cu - \alpha - Fe_2O_3$ nanocomposite. The observed non-uniformity in the crystalline structure may significantly influence the material's physical and chemical properties (Kamal et al., 2023). Understanding these characteristics is crucial for optimizing the nanocomposite performance in various applications. However, The SEM images indicate irregularities in the crystalline structure. This non-uniformity can affect how the nanocomposite interacts with other materials, potentially influencing its catalytic efficiency and reactivity (Diliraj 2022). The geometry of the particles varies throughout the sample. Such variations can lead to differences in surface area and porosity, which are critical factors in photocatalysis applications. Such unique characteristics of the $Cu - \alpha - Fe_2O_3$nanocomposite suggest potential uses in areas such as heterogeneous catalysis, where a larger surface area and specific geometric configurations can enhance reaction rates.

The typical FTIR spectrum of the synthesized nanocomposite (Fig. 6) displayed various peaks at 426, 693, 849, 916, 949, 1457, 1543, 1651, 1994, 2102, 2318, 2847, 2992, 3332, 3442, and 3529 cm^{-1}. The peaks at 849 cm^{-1}, 916 cm^{-1}, and 949 cm^{-1} correspond to Fe—O bond stretching vibrations In contrast, the peaks at 426 cm^{-1} and 693 cm^{-1} are attributed to bond stretching vibrations due to CuO, these confirmed the presence of $CuO$and$\alpha - Fe_2O_3$groups in the sample (Darma et al., 2019). Additionally, the stretching vibrations of the O—H bond are noted at 3447 cm^{-1}, while the symmetric stretching vibrations of the O—H bond appear at 3332 cm^{-1}. The presence of an adsorbed hydroxide group is indicated by the peak at 2922 cm^{-1}. These findings suggest that some water molecules are present in the sample. The FTIR analysis provides valuable insights into the functional groups and molecular interactions within the synthesized nanocomposite, reinforcing its potential applications in fields.

Comparative Study of MO Degradation Using CuO,$\alpha - Fe_2O_3$ and $CuO - \alpha - Fe_2O_3$nanocomposite

The performance of the $CuO - \alpha - Fe_2O_3$ nanocomposite was compared to the pure forms of CuO and α-Fe_2O_3. According to the experimental results presented in Fig. 7, the percentage of methyl orange (MO) degradation estimated using the CuO-α-Fe_2O_3 nanocomposite was 71.6%. In contrast, the degradation percentages for pure CuO and α-Fe_2O_3 were 26.4% and 34.8%, respectively. These findings suggest that the $CuO - \alpha - Fe_2O_3$ nanocomposite exhibits significantly higher photocatalytic activity compared to its pure components, CuO and α-Fe_2O_3. According to Pan et at., (2013), $\alpha - Fe_2O_3$is an n-type semiconductor with an energy band gap (Eg) of 2.1 eV, while CuO is a p-type semiconductor with an Eg of 1.21 eV. This difference allows for the formation of a p-n junction, which enhances the visible-light photocatalytic activity of the hybrid oxide catalyst. Under identical experimental conditions specifically, a catalyst dose of 0.2 g, a methyl orange (MO) concentration of 30 mg/L, a pH of 6, and a 15-minute irradiation interval using a 500W halogen lamp. The produced $CuO - \alpha - Fe_2O_3$ nanocomposite, along with pure samples of both CuO and $\alpha - Fe_2O_3$semiconductors, were tested for the degradation of methyl orange. The data presented in Figure 7 clearly demonstrate that the decomposition of methyl orange increased significantly with the use of the hybrid catalyst.

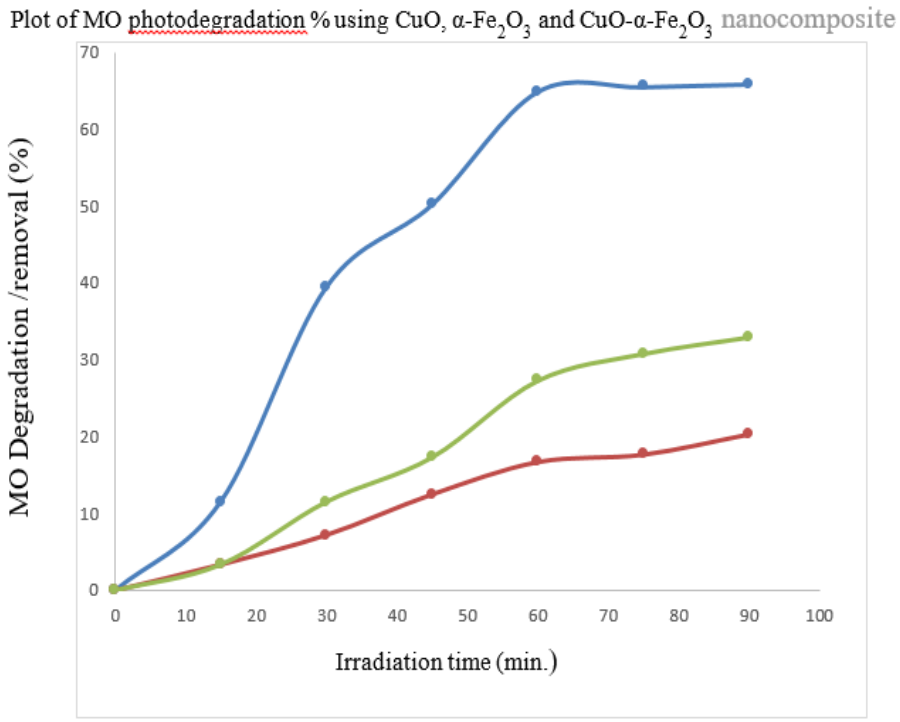

Figure 7: Plot of comparative study ofCuO,$\alpha - Fe_2O_3$and$CuO - \alpha - Fe_2O_3$Photocatalysis

Photocatalytic activity test for the degradation of MO

The photocatalytic degradation of methyl orange (MO) was investigated at room temperature under specific experimental conditions: (30 mg/L MO, a dosage of 0.2 g, and a pH of 6). A 500W halogen bulb used as the visible light source throughout the experiment in Figure 5. As the duration of irradiation increased, the rate of MO degradation also rose until a steady state was reached where the relative absorbance of MO showed minimal change. To analyse this behaviour, a graph of ln[Co/C] against irradiation time was constructed based on the pseudo-first-order kinetics (Fig. 7). The linear relationship between the reaction rate and time signifies that the photocatalytic process follows pseudo-first-order kinetics. The study effectively highlights the relationship between irradiation time and the rate of degradation of the MO, confirming that the degradation process adheres to pseudo-first-order kinetics. The results suggest that the photocatalytic method employed is efficient for the degradation of MO under the specified experimental conditions.

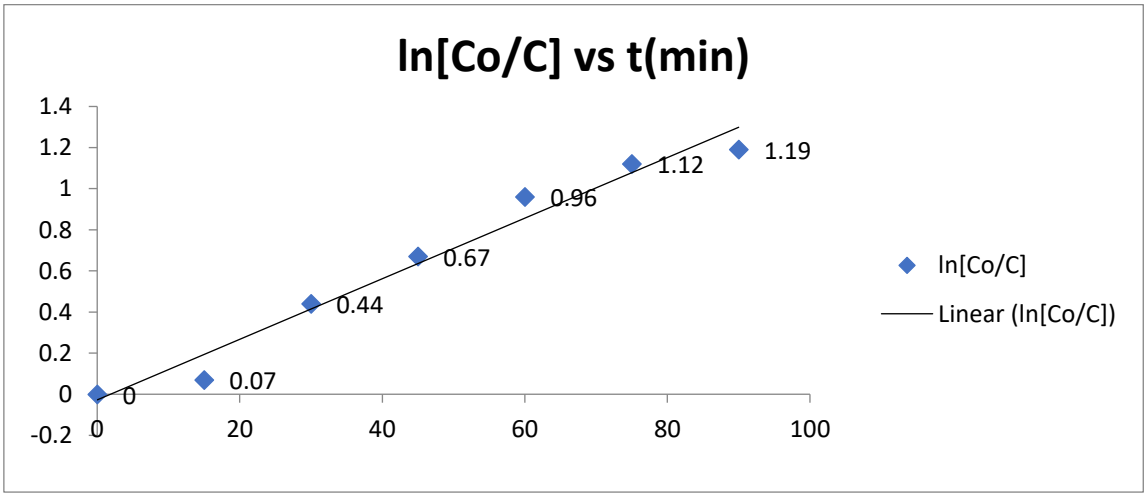

Figure 8: Plot of the rate of MO degradation against the irradiation time

Kinetics study of the reaction

The photocatalytic destruction of organic contaminants requires the involvement of both organic molecules and oxygen. Given the abundance of oxygen in the environment, we can reasonably assume that, its concentration remains relatively constant throughout the photocatalytic process (Liu et al., 2014). According to the law of mass action, the photocatalytic reaction behaves as a quasi-first-order reaction. The rate of the photocatalytic process can be expressed as eq. (2):

$$r = \frac{-\partial c_{(t)}}{\partial t} = k_{c(t)} \qquad (2)$$

Where $C_{(t)}$ represents the concentration of methyl orange (MO) adsorbed at time (t), and (k_c) is the rate constant. However, the photocatalytic degradation process is fundamentally reliant on the effective adsorption of MO onto

the$CuO-\alpha-Fe_2O_3$nanocomposite surface. The assumption of a Langmuir isotherm for the adsorption-desorption equilibrium provides a solid foundation for understanding this process. Thus eqn. (2) can be modified to eqn. (3) when the A–D equilibrium is satisfied during photocatalytic processes under visible light irradiation.

$$r = \frac{k_c k_{ad} C}{1+k_{ad} C} = k_{c(t)} \quad (3)$$

k_{ad} is the A–D equilibrium constant, C is MO concentration in solution at time t. However, for effective degradation conditions, the MO concentration should be low, and hence the $K_{ad}C$ in eqn (3) is significantly lower than 1, and it changes to eqn (4)

$$r = -\frac{\partial C}{\partial t} = k_c k_{ad} C = k_{app} C \quad (4)$$

k_{app} is the apparent rate constant obtained by multiplying kc and kad. Hence integrating the eq. (4) from time t_o to time t. gives another form of the L–H model eqn (5)

$$ln\left[\frac{C_o}{C_t}\right] = k_{app} t \quad (5)$$

Where Co represents the MO concentration at time 0 and Ct represents the concentration at time t during the photocatalytic process. The kapp of MO photocatalytic degradation can be simply calculated using eqn (5). It was also reported by Liu et al., (2014) that, the concentration of the MO absorbed on the $CuO-\alpha-Fe_2O_3$ surface can be calculated using the steady-state method in which adsorption equals the total of desorption and reaction. Thus the $C_{(t)}$ in equation (2), becomes

$$C_{(t)} = \frac{k_a[X_s]C}{k_d+k_a C+k_c C} \quad (6)$$

Where [Xs] is the absorption site density on the surface of the photocatalysis, ka and kd are the adsorption-desorption rate (A–D) equilibrium constant. It can be seen that the C(t) under steady state conditions is lower than the concentration at A–D equilibrium, as compared to eqn (3). The effect of the photocatalytic reaction on the A–D equilibrium can be ignored for low photocatalytic activity, and eqn (6) can be reduced to eqn (4). However, according to Kim et al., (2008), the expression for the rate of photocatalytic degradation of organic substrates

Mechanism of the Degradation reaction

The MO dye absorbs visible light of an appropriate wavelength (465) and produces an excited singlet state, which then undergoes inter system crossing (ISC) to produce the MO triplet state. The semiconducting CuO-Fe_2O_3, on the other hand, uses irradiated light energy to excite its electrons from the balance band (VB) to the conduction band (CB), resulting in a hole (h^+), which withdraws electrons from the available hydroxyl ions (HO^-) to generate hydroxyl radicals ($HO^\bullet$), which interact with the MO triplet state to produce MO/Intermediate, followed by the degradation of the MO to the final products.

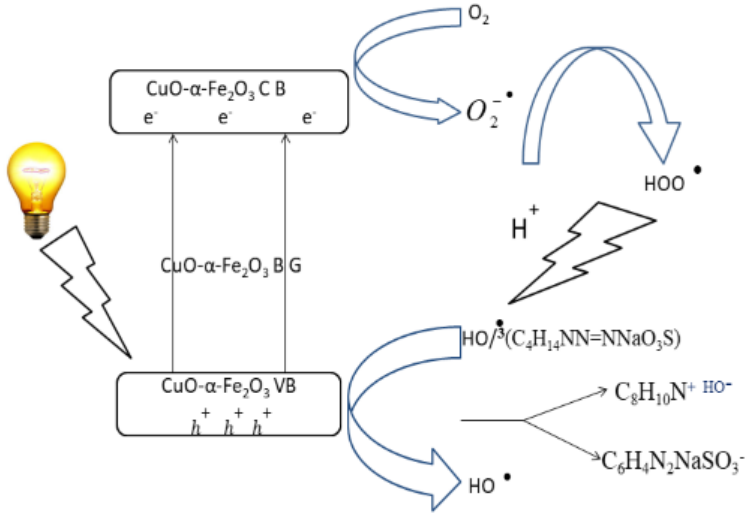

Figure 9: Proposed mechanism for the MO degradation

CONCLUSION

Co-precipitation was employed to synthesize the CuO-α-Fe_2O_3 nanocomposite. Scanning Electron Microscopy (SEM), X-ray Diffraction (XRD), and Fourier Transform Infrared Spectroscopy (FT-IR) analyses reveal distinct phases within the nanocomposite, including hematite and monoclinic nanoparticles, along with indications of potential copper ferrite formation. These findings highlight the complex structural characteristics of the synthesized material and suggest its promising applications across various fields. The photocatalytic activity of the nanocomposite was further investigated using methyl orange as a model dye effluent. Under visible light, the CuO-α-Fe_2O_3 nanocomposite demonstrated exceptional photocatalytic performance, achieving a degradation efficiency of 71.6% within 1.5 hours. In comparative tests, the pure forms of CuO and Fe_2O_3 were evaluated, showing approximately a 50% improvement in degradation efficiency when combined in the nanocomposite compared to their individual components. A kinetic study of the reaction indicates that the degradation process follows pseudo-first-order kinetics. This suggests that the rate of reaction is directly proportional to the concentration of the dye, which is a crucial factor in evaluating the effectiveness of the photocatalyst. The development of the CuO-α-Fe2O4 nanocomposite represents a significant advancement in photocatalytic technology for wastewater treatment. Its impressive degradation performance, demonstrated through the methyl orange test, underscores its potential application in real-world scenarios..

RECOMMENDATIONS

The photocatalytic degradation of azo dyes in wastewater treatment encompasses a broad array of topics. There are several areas in which the application of $CuO-\alpha-Fe_2O_3$ nanocomposite materials for photocatalytic degradation could be further explored are:

In this study, a model dye (methyl orange) was potocatalytically removed by visible light irradiation, and the degree of decolorization was measured. Textile waste water, on the other hand, may contain a mixture of colors, inorganic ions, humic acid, and various types of solvent as typical constituents, necessitating additional research in this area. This will be a necessary step in scaling up the photocatalytic water treatment process.

A batch system experiment using a slurry type was used in this study. Although catalyst recovery and regeneration is an unavoidable stage in the waste water treatment process, the produced $CuO-\alpha-Fe_2O_3$ nanocomposite performance and durability have not been fully evaluated. This necessitates additional research in this area.

The activity of $CuO-\alpha-Fe_2O_3$ that was produced was tested on a laboratory scale. Weather variables like as wind, temperature, humidity, UV light, and others, on the other hand, may have an impact on its activity. As a result, more research should be done in this area in order to turn $CuO-\alpha-Fe_2O_3$ into a comprehensive model photocatalyst for waste water treatment at industrial scale.

It is necessary to investigate the possibility of using photocatalysis in an existing waste water treatment plant. When combined with other new water treatment technologies, photocatalysis may provide synergistic benefits.

REFERENCES

Abdulhamid H., Israila J. J., Bello M., (2017). Enhanced photocatalytic activity of calcined natural sphalerite under visible light irradiation, m a t e r r e s t e c h n o l; 6(1):1 6.

Auwal Y., Darma M.S., and Kamaluddeen A. I. (2023). Sol-gel synthesis of ZnO nanoparticles for optmized photocatalytic degradation of Eriochrome Black T under UV irradiation. *Algerian Journal of Engineering and Technology*. Vol 08 pp117–130.

Byrappa, K., Subramani, A. K., Ananda, S., Lokanatha Rai, K. M., Dinesh, R., & Yoshimura, M. (2006). Photocatalytic degradation of rhodamine B dye using hydrothermally synthesized ZnO. *Bulletin of Materials Science*, *29*(5), 433–438. https://doi.org/10.1007/BF02914073

Casbeer, E., Sharma, V. K., & Li, X. Z. (2012). Synthesis and photocatalytic activity of ferrites under visible light: A review. *Separation and Purification Technology*, *87*, 1–14. https://doi.org/10.1016/j.seppur.2011.11.034

Chen, P., Xing, X., Xie, H., Sheng, Q., & Qu, H. (2016). High catalytic activity of magnetic CuFe 2 O 4 / graphene oxide composite for the degradation of organic dyes under visible light irradiation. *Chemical Physics Letters*, *660*, 176–181. https://doi.org/10.1016/j.cplett.2016.08.020

Diliraj Upadhaya and Debarun Dhar Purkayastha. (2022). Self-cleaning activity of CuO/ZnO heterostructure: A synergy of photocatalysis and hydrophilicity. *Journal of the Taiwan Institute of Chemical Engineers.* Volume 132. https://doi.org/10.1016/j.jtice.2022.104216

Hamza, A., J.T, F., Waziri, S. ., & Ajayi, O. . (2013). Solar photocatalytic degradation of phenol using nanosized ZnO and -Fe2O3. *Journal of Chemical Engineering and Materials Science*, *4*(7), 87–92. https://doi.org/10.5897/JCEMS2013.0162

Hamza, A., John, I. J., & Mukhtar, B. (2017). Enhanced photocatalytic activity of calcined natural sphalerite under visible light irradiation. *Journal of Materials Research and Technology*, *6*(1), 1–6. https://doi.org/10.1016/j.jmrt.2016.03.001

H. Kumari, S. Suman, R. Ranga, S. Chahal, S. Devi, S. Sharma, S. Kumar, P. Kumar, A. Kumar and R. Parmar. (2023). A Review on Photocatalysis Used For Wastewater Treatment: Dye Degradation. Water, Air, and Soil Pollution Vol. 234

Kabo KS, Yacob AR, Darma MS, Michael BO, Alisi IO, Bello AM. (2023). Morphological effect of surface modified, nanoflower and nanotube zinc oxide catalysts for biodiesel production. Discovery 2023; 59: e37d1036

Liu, B., Zhao, X., & Terashima, C. (2014). Thermodynamic and kinetic analysis of heterogeneous photocatalysis for, 8751–8760. https://doi.org/10.1039/c3cp55317e

M.S. Darma, Y. Auwal and A. Aminu (2019). Photocatalytic activity, optimization and modelling of Fe_2O_3/CuO mixed composite for the removal of organic dyes by visible light illumination. *Records of Chemical Science (FRsCS).* Vol. 1 (2) pp 74–85. https://api.semanticscholar.org/CorpusID:214501281

Pan, L., Tang, J., & Wang, F. (2013). Facile synthesis of nanoscaled α-Fe2O3, CuO and CuO/Fe2O3hybrid oxides and their electrocatalytic and photocatalytic properties. *Central European Journal of Chemistry*, *11*(5), 763–773. https://doi.org/10.2478/s11532-013-0207-6

Sani Muhammad, Muhammad Suleiman Darma and Al-Amin Bashir (2024). Synthesis and characterization of salicylaldehyde and 2,4-dinitrophenyl hydrazine schiff base with its cobalt (ii) and manganese (ii) complexes. *FUDMA Journal of Sciences (FJS)* Vol. 8 No. 4, pp 333–337.

Singh, K., Bharose, R., Verma, S. K., & Singh, V. K. (2013). Potential of powdered activatedmustard cake for decolorising raw sugar. *Journal of the Science of Food and Agriculture*, *93*(1), 157–165. https://doi.org/10.1002/jsfa.5744

Taylor, P., Gotostos, M. J. N., Su, C. C., De, M. D. G., & Lu, M. (2014). Kinetic study of acetaminophen degradation by visible light photocatalysis Kinetic study of acetaminophen degradation by visible light photocatalysis. Journal of Environmental Science and Health. 211, 37–41. https://doi.org/10.1080/10934529.2014.894310

Umar Bilal, Ibrahim Imrana and Muhammad Suleiman Darma (2020). Gravimetric determination of sulphate in some selected industrial effluents. *FUDMA Journal of Sciences* Vol. 4 No.4, pp 290 - 294. DOI: https://doi.org/10.33003/fjs-2020-0404-512

Vinodgopal, K., & Kamat, P. V. (1995). Enhanced Rates of Photocatalytic Degradation of an Azo Dye Using SnO2/TiO2Coupled Semiconductor Thin Films. *Environmental Science and Technology*, *29*(3), 841–845. https://doi.org/10.1021/es00003a037

Zhang, G., Liu, H., Cooper, A. T., & Wu, R. (2007). CuFe 2 O 4 / activated carbon composite : A novel magnetic adsorbent for the removal of acid orange II and catalytic regeneration, *68*, 1058–1066. https://doi.org/10.1016/j.chemosphere.2007.01.081